Desalination and Water Treatment
www.deswater.com
doi: 10.1080/19443994.2013.856346

53 (2015) 1862–1880
February

Taylor & Francis
Taylor & Francis Group

Modeling of nitritation and denitritation in a novel PITSF-SEU process using an extension of ASM2d model

Rusul Naseer Mohammed[a,b], L. Xiwu[a,*]

[a]*School of Energy and Environment, Southeast University, Sipailou Road, Nanjing 210096, PR China*
Tel. +86 13276577810; email: alotito@yahoo.com
[b]*Faculty of Engineering, Chemical Engineering Department, University of Basrah, Basra, Iraq*

Received 20 April 2013; Accepted 8 October 2013

ABSTRACT

In this study, an anaerobic–anoxic/oxic (A2/O) multiphased biological process called "phased isolation tank step feed technology of southeast university (PITSF-SEU)" was developed to force the oscillation of organic and nutrient concentrations in process reactors. PITSF reactor is effective for reducing energy consumption because it does not contain the internal recycle of mixed liquor and sludge return device. A computer program was built based on mass balance equations on each tank using an extension activated sludge model for simulating the soluble and particulate compounds in each tank of PITSF-SEU system. The considerable differences between the extension model and other models are two stage for nitrification process and multistage for denitrification process. Also, phosphorus removal was taken into account simultaneously in this model. The difficulty of model simulation is coming from the system operation with unsteady-state condition and the changing of multipoint step feed location with its phase time. Also, there are some tanks in PITSF SEU process are operated under combined effect of nitrification and denitrification (SND) which makes difficulty in the reaction calculation. The results showed that the growth rate constants of X_{AOB} and X_{NOB} were 1.4 and 0.4 d^{-1}, respectively. Y_{AOB} value was 0.14, and Y_{NOB} value was 0.04. It was showed a good agreement between the observed and simulated data, whereas the sum of squares of the deviations (R^2) of soluble components S_{NH4}, S_{PO4}, S_{NO3}, and S_{NO2} were more than 0.95 in all investigated runs. According to extension model simulation, the biomass concentration of X_H, X_{PAO}, X_{PP}, X_{AOB}, and X_{NOB} was decreased in the anaerobic tanks because of the lysis reaction. Then, the X_H, X_{PAO}, X_{PP}, X_{AOB}, and X_{NOB} was increased in the aerobic tanks due to aerobic growth.

Keywords: PITSF-SEU; N–P removal; Mathematical model; Microbial kinetic behaviors

1. Introduction

Increasing requirement for nutrient removal during the last decade has led to more complex wastewater treatment processes. Currently, a variety of activated sludge processes have been employed for nutrient removal. One of the widely used BNR processes is the anaerobic, anoxic, and aerobic process (A2/O). The operational cost of A2O process is high due to needing reflow recycling devices of mixed liquor and sludge. Therefore, The A2O process was reconfigured

*Corresponding author.

into six compartments with multiphased that is called phased isolation tank step feed process (PITSF-SEU). This process was invented in southeast university, and it has been published in our previous study [1]. It was designed like SBR in control methodology and AA/O in spatial structure. Indeed, it is more similar to a normal multitank process, such as A2/O or UCT, but the operational cost of PITSF-SEU is low compared with A2O and UCT process because the operation cost was minimized through omitting the mixed liquor and sludge recycles devices. The direction of flow in this system is changed automatically through changing intake location. In order to understand bacterial conversion in BNR processes and for the optimization of nutrient removal, mathematical modeling and simulation became popular in recent years, and many different types of mathematical models have been proposed [2,3] and applied in the biological nutrient removal processes. Operational scenarios may be tested by simulation rather than conducting trial and error experiments at full scale. To date, the most successful model is activated sludge model No. 1 (ASM1), which is developed in 1986 by the task group for mathematical modeling [4]. ASM1 has been extended to include a description of biological phosphorus removal, resulting in ASM2 [5,6] and ASM2d [7,8]. Recently, some of the model concepts behind ASM1 have been altered in ASM3 [9,10] which also focus on the degradation of carbon and nitrogen. It is well known that influent organic substrate is a key component for denitrification and biological phosphorus removal. If the organic loading is less, remaining nitrate from the preceding cycle affects the phosphorus release in the next feed phase. A significant portion of organic loading was utilized for denitrification. Therefore, the availability of biodegradable carbon for phosphorus-accumulating organisms (PAO) will be reduced which caused a deterioration in biological phosphorus removal. Additionally, the nitrification process was assumed to be a one-stage process [11,12], directly from ammonia (S_{NH4}) to nitrate (S_{NO3}) in these models. The nitrifying bacteria species were not divided into two species, ammonia-oxidizing bacteria (AOB, X_{AOB}) and nitrite-oxidizing bacteria (NOB, X_{NOB}). In addition, denitrification was also assumed to be a one-stage process, directly from S_{NO3} to nitrogen gas. The discussion of nitrite (S_{NO2}) variation was absent in these models. Since nitrogen removal is one of the aims of BNR process, simulation of X_{AOB}, X_{NOB}, and oxidized nitrogen (S_{NO2} and S_{NO3}) becomes important on operation and management of BNR process. In this study, an extension activated sludge model was established in PITSF-SEU process that considered not only the kinetics and stoichiometry of X_{AOB} and X_{NOB} but also the reduction of S_{NO2} and S_{NO3}. The objectives of this study are listed as follows: (1) to establish an extension model for describing the transformation of different components including carbon, nitrogen, and phosphorus in the PITSF-SEU process, (2) to determine the kinetic parameters of two nitrifying species X_{AOB} and X_{NOB} using oxygen uptake rate (OUR) batch experiments, (3) to explore the consistency between simulation and observed values of different soluble and particulate components such as, S_{NH4}, S_{NO2}, S_{NO3} and orthophosphate (S_{PO4}), and (4) to analyze the kinetics of different micro-organisms, including X_H, X_{PAO}, X_{pp}, X_{PHA}, X_{AOB}, and X_{NOB} in PITSF-SEU process under different runs.

2. Materials and methods

2.1. Treatment plant configuration

Laboratory experiments were conducted in a new pilot scale of PITSF-SEU that composed of a rectangular box divided by baffles to form six-tank reactor. All tank except the last one have the same rectangular plane of 280 mm × 240 mm and supplied with mechanical mixers and air diffusers for providing a suitable state condition (anaerobic–anoxic/oxic) in a same tank. The last tank was operated as a clarifier. The particular advantages of this process, it has a simple structure, compact volume and operated safely. This process is a continuous flow process with a constant water level that makes high utilization capacity in the system. The main parts of a pilot plant utilized in this study are the main body that is a rectangular box of 860 mm × 535 mm × 905 mm, prestatic pumps, PLC programmable logic control, LCD display screen, inlet wastewater electromagnetic valves, outlet water, PVC pipes and others. The principle diagram of pilot plant with all major components is shown in Fig. 1. The effective water depth in the PITSF-SEU process is 700 mm, while the total depth is 900 mm. An operation cycle is composed of two half-cycles with same running schemes as shown in Fig. 2. It is divided into six phases named as phase I, II, and III during the first half-cycle and phase IV, V, and VI during the second half-cycle. An optimized removal efficiency of pollutant was achieved at a HRT of 15 h, SRT of 13 day, aeration ratio of 10% at a temperature range of 11–21℃ and sludge recycle ratio of 35%. The optimized running time was 3, 2.5, and 2 h of phase I, II, and III, respectively.

2.2. Analytical methods

COD, ammonia–N, nitrate–N, nitrite–N, PO_4–P, TP, and TN were analyzed according to standard

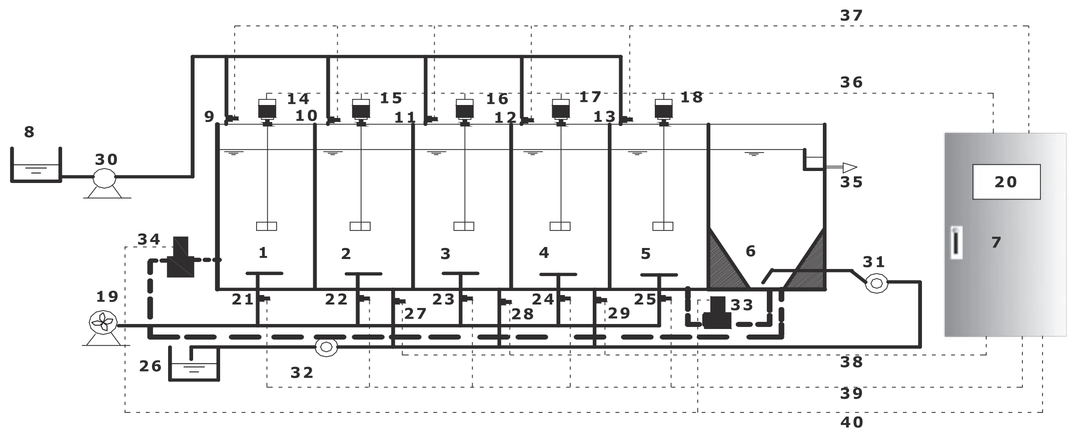

Fig. 1. Configuration of PITSF-SEU system with all main parts, 1–5, five tank; 6, settling tank; 7, PLC programmable logic controller; 8, feed tank; 9–13, inlet electromagnetic valve; 14–18, mixer; 19, air compressor; 20, touch screen of control panel; 21–25, aeration electromagnetic valve; 26-excess sludge tank 27, 28, 29; sludge return valve; 30, inlet prestatic pump; 31, sludge recycle control meter; 32, excess sludge control meter; 33–34, sludge discharge valves; 35, effluent; 36, electrical mixer line; 37, electrical inlet valve line; 38, electrical sludge return valve line; 39, electrical aeration valve line; 40, electrical sludge discharge valve line.

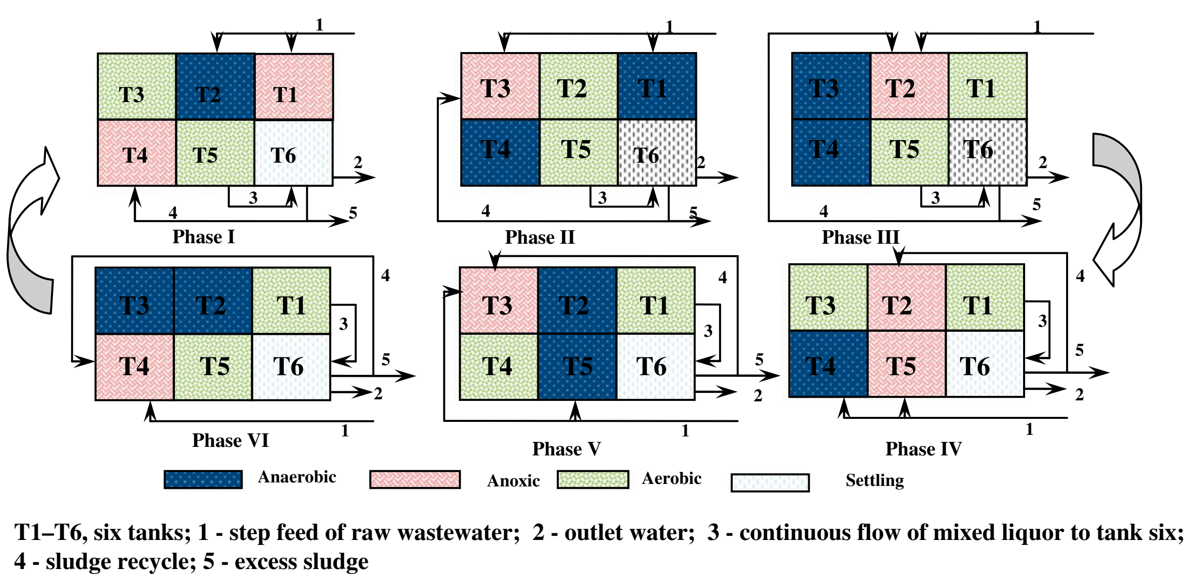

Fig. 2. Run scheme of PITSF-SEU activated sludge system [1].

methods [13]. Nitrate–N were analyzed by the IC method (Metrohm 761 compact IC equipped with Metrosep A Supp 5 column and TN was analyzed by Analytik Jena AG multi N/C 3000.

2.3. Determination of COD fraction and OUR experiments

Several methods have been developed for wastewater characterization, but the two most commonly used processes are the biological and physical/chemical characterizations. The physicochemical method is based on the assumption that COD fractions model can be separated by filtration and flocculation processes and that COD of the gained fractions is easily measurable by standard chemical methods [14]. In this study, wastewater characterization was determined by physicochemical method for determining COD fraction as explained in Fig. 3, which depicts the retention or passage of the influent wastewater COD components through sequential 1.2 μm-glass-fiber filtration, flocculation (to remove colloidal matter from liquid phase) and 0.45 μm-membrane filtration. The main steps and theoretical formulas of COD fractionation are shown below:

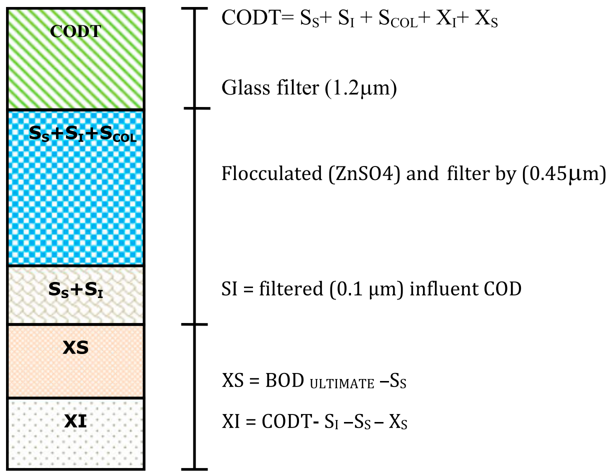

Fig. 3. Summary of influent characterization for organic wastewater components.

S_I = 90% of filtered (0.45 μm) effluent COD or S_I = filtered (0.1 μm) influent COD.

S_S = Flocculated ($ZnSO_4$) and filtered (0.45 μm) influent COD–S_I.

$S_F = S_S–S_A$; $X_S = BOD_{ULTIMATE}–S_S$; and $X_I = COD_T–S_I–S_S–X_S$.

In addition, OUR was used to calculate the biomass of X_H, X_{AOB}, and X_{NOB} in a raw wastewater. It refers to the amount of oxygen used by a unit mass of active sludge in a unit of time. A certain quantity of MLSS sample was taken from Wuxi wastewater and added into OUR chambers. In order to evaluate the kinetic parameters and active biomass of X_H, X_{AOB}, and X_{NOB}, different types of OUR values should be considered:

Total OUR (OUR_T); OUR of X_H (OUR_H); OUR of X_{AOB} (OUR_{AOB}) and OUR of X_{NOB} (OUR_{NOB}). The determination of OURs of X_H; X_{AOB} and X_{NOB} were based on the subsequent addition of allylthiourea (ATU) and NaN_3, selective inhibitors of X_{AOB} and X_{NOB}, to the MLSS sample. As determining OUR_T, no inhibitor was added. When determining OUR_H, both allylthiourea (86 μM) and NaN3 (24 μM) [15] were added. If only NaN3 (24 μM) was added, the determined OUR was the sum of OUR_H and OUR_{AOB}, then

$OUR_{NOB} = OUR_T − (OUR_H + OUR_{AOB})$.

$OUR_{AOB} = (OUR_H + OUR_{AOB}) − OUR_H$.

The raw wastewater was typical in Wuxi campus of southeast university, China. COD unfiltrated was fluctuated between 175 and 700.2 mg/L with an average of 575 mg/L, of which S_S, S_I, X_S and X_I accounted for about 38, 2, 43 and 11%, respectively. MLSS was between 45 and 93 mg/L with average of 76 mg/L. NH_4^+-N was between 16 and 46 mg/L with average of 28 mg/L. TP was between 1.5 and 4.7 mg/L with an average of 3.2 mg/L, of which PO_4^{3-}–P accounted for about 74–93%.

2.4. Mass balance equations and model algorithms

A computer program called "extension of ASM2d model" was built based on mass balance equations on each tank of PITSF-SEU system after solving the differential equation by Euler method. Model configuration of the PITSF-SEU system during a first half-cycle is explained clearly in Fig. 4. The algorithm for implementing the calculation of extending activated sludge model was described as follows:

Inlet−Outlet + Reaction rate = Accumulation

$$QC_{0,j} + r_j V = QC_{2i,j} + V\frac{dC_{i,j}}{dt} \tag{1a}$$

$$C(t) \times \left(\frac{dc}{dt}\right) = \frac{C_{0i,j} - C_{i,j} + M_{i,j} - N_{i,j}}{V_{i,j}\, C_{i,j}} \tag{1b}$$

where Q: inlet flow rate; V: volume of each tank; r: reaction rate where it was calculated according to extending activated sludge model; $C_{2i,j}$: component concentration in the reaction tanks, i = 1, 2, 3, i.e. tank number; j = component number; $C_{0,j}$: influent concentration (MT^{-1}); $C_{i,j}$: effluent concentration.

$M_{i,j}$, $N_{i,j}$ are production and consumption (MT^{-1}) terms of the j No. component in the i No. tank.

(1) During Phase I, the mass balance equations can be written (from Fig. 5(a)) as:

Tank no. 1:

$$0.5 \times Q \times (C_0 - C_1) + r_1 \times V = V \times \frac{dC_1}{dt} \tag{2}$$

Tank no. 2:

$$0.5 \times Q \times (C_0 + C_1) - Q \times C_2 + r_2 \times V = V \times \frac{dC_2}{dt} \tag{3}$$

Tank no. 3:

$$Q \times C_2 - Q \times C_3 + r_3 \times V = V \times \frac{dC_3}{dt} \tag{4}$$

Tank no. 4:

$$Q \times C_3 + Qr \times Cr - (Q + Qr) \times C_4 + r_4 \times V = V \times \frac{dC_4}{dt} \tag{5}$$

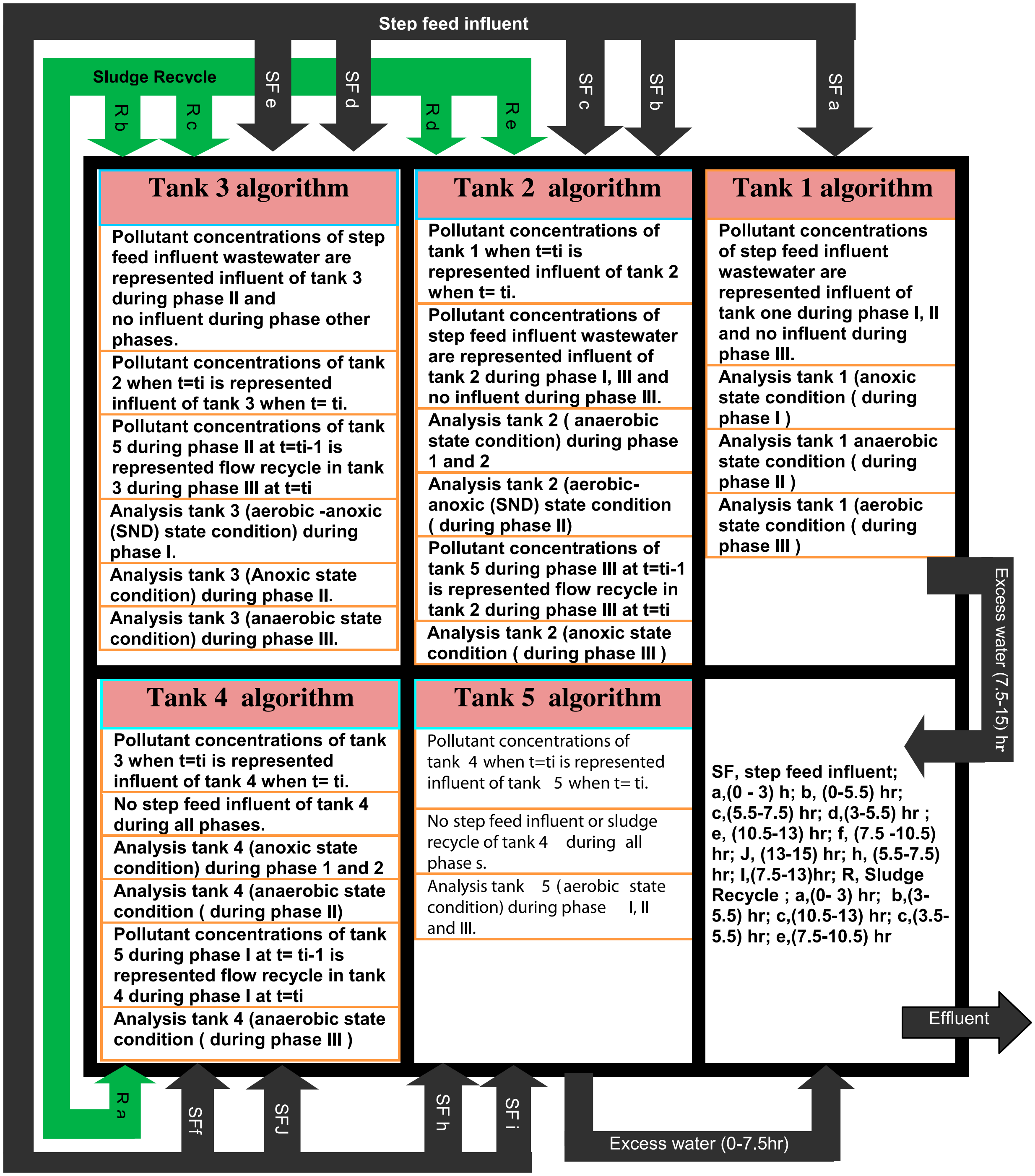

Fig. 4. Layout and algorithms of PITSF-SEU process during a first half cycle.

Tank no. 5:

$$(Q + Qr) \times C_4 - (Q + Qr) \times C_5 + r_5 \times V = V \times \frac{dC_5}{dt} \quad (6)$$

(1) During Phase II, the mass balance equations can be written (from Fig. 5(b)) as:

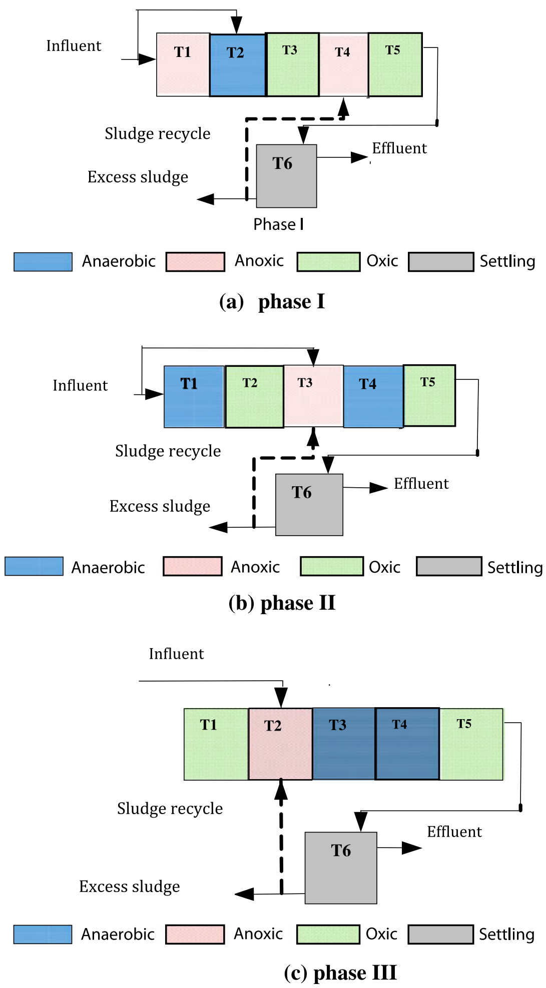

Fig. 5. Diagram of mass balance equation during all phases.

Tank no. 1:

$$0.5 \times Q \times (C_0 - C_1) + r_1 \times V = V \times \frac{dC_1}{dt} \tag{7}$$

Tank no. 2:

$$0.5 \times Q \times (C_1 - C_2) + r_2 \times V = V \times \frac{dC_2}{dt} \tag{8}$$

Tank no. 3:

$$0.5 \times Q \times (C_0 + C_2) + Qr \times Cr - (Q + Qr) \times C_3 + r_3 \times V = V \times \frac{dC_3}{dt} \tag{9}$$

Tank no. 4:

$$(Q + Qr) \times C_3 - (Q + Qr) \times C_4 + r_4 \times V = V \times \frac{dC_4}{dt} \tag{10}$$

Tank no. 5:

$$(Q + Qr) \times C_4 - (Q + Qr) \times C_5 + r_5 \times V = V \times \frac{dC_5}{dt} \tag{11}$$

(1) During Phase III, the mass balance equations can be written (from Fig. 5(c)) as; Tank no. 2:

$$Q \times C_0 + Qr \times Cr - (Q + Qr) \times C_2 + r_2 \times V = V \times \frac{dC_2}{dt} \tag{12}$$

Tank no. 3:

$$(Q + Qr) \times C_2 - (Q + Qr) \times C_3 + r_3 \times V = V \times \frac{dC_3}{dt} \tag{13}$$

Tank no. 4:

$$(Q + Qr) \times C_3 - (Q + Qr) \times C_4 + r_4 \times V = V \times \frac{dC_4}{dt} \tag{14}$$

Tank no. 5:

$$(Q + Qr) \times C_4 - (Q + Qr) \times C_5 + r_5 \times V = V \times \frac{dC_5}{dt} \tag{15}$$

where Qr = flow rate of sludge recycle and its value 35% of influent flow rate; V = 47 L the volume of each tank.

The reaction rate (r_i) is calculated by summing the product of the process rate expression (ρ_j) (Table 1) and the stoichiometric coefficients $V_{i,j}$ (Table 2) for the component (No. i) being considered in the mass balance:

$$r_i \sum_j v_{i,j}\ \rho_j \tag{16}$$

The equations that described the transformation of the wastewater quality in the extension model produced an ordinary differential equations system. Then, the set of equations were integrated simultaneously by the first-order Euler numerical method. The entire model was implemented by means of a computer program that was coded with MATLAB 2010 language

Table 1
Process rate equation of extension model

j	Process	Process rate equation $\rho_j, \rho_j \geq 0$ $(M_1\ L^{-3}\ T^{-1})$
Heterotrophic organisms: X_H		
1	Aerobic growth on S_F	$\mu_H \frac{S_{O2}}{K_{O2H}+S_{O2}} \frac{S_F}{K_{FH}+S_F} \frac{S_F}{S_A+S_F} \frac{S_{NH4}}{K_{NH4H}+S_{NH4}} \frac{S_{PO4}}{K_{PH}+S_{PO4}} \frac{S_{ALK}}{K_{ALKH}+S_{ALK}} X_H$
2	Aerobic growth on S_A	$\mu_H \frac{S_{O2}}{K_{O2H}+S_{O2}} \frac{S_F}{K_{FH}+S_F} \frac{S_A}{K_{AH}+S_A} \frac{S_A}{S_A+S_F} \frac{S_{NH4}}{K_{NH4H}+S_{NH4}} \frac{S_{PO4}}{K_{PH}+S_{PO4}} \frac{S_{ALK}}{K_{ALKH}+S_{ALK}} X_H$
3	Anoxic growth on S_F, denitrification (S_{NO2})	$\mu_H \eta_{NO2H} \frac{K_{O2H}}{K_{O2H}+S_{O2}} \frac{S_{NO2}}{K_{NO2H}+S_{NO2}} \frac{S_F}{K_{FH}+S_F} \frac{S_F}{S_A+S_F} \frac{S_{NH4}}{K_{NH4H}+S_{NH4}} \frac{S_{PO4}}{K_{PH}+S_{PO4}} \frac{S_{ALK}}{K_{ALK}+S_{ALK}} X_H$
4	Anoxic growth on S_F, denitrification (S_{NO3})	$\mu_H \eta_{NO3H} \frac{K_{O2H}}{K_{O2H}+S_{O2}} \frac{S_{NO3}}{K_{NO3H}+S_{NO3}} \frac{S_F}{K_{FH}+S_F} \frac{S_F}{S_A+S_F} \frac{S_{NH4}}{K_{NH4H}+S_{NH4}} \frac{S_{PO4}}{K_{PH}+S_{PO4}} \frac{S_{ALK}}{K_{ALK}+S_{ALK}} X_H$
5	Anoxic growth on S_A, denitrification (S_{NO2})	$\mu_H \eta_{NO2H} \frac{K_{O2H}}{K_{O2H}+S_{O2}} \frac{S_{NO2}}{K_{NO2H}+S_{NO}} \frac{S_A}{K_{AH}+S_A} \frac{S_A}{S_A+S_F} \frac{S_{NH4}}{K_{NH4H}+S_{NH4}} \frac{S_{PO4}}{K_{PH}+S_{PO4}} \frac{S_{ALK}}{K_{ALK}+S_{ALK}} .X_H$
6	Anoxic growth on S_A, denitrification (S_{NO3})	$\mu_H \eta_{NO3H} \frac{K_{O2H}}{K_{O2H}+S_{O2}} \frac{S_{NO3}}{K_{NO3H}+S_{NO3}} \frac{S_A}{K_{AH}+S_A} \frac{S_A}{S_A+S_F} \frac{S_{NH4}}{K_{NH4H}+S_{NH4}} \frac{S_{PO4}}{K_{PH}+S_{PO4}} \frac{S_{ALK}}{K_{ALK}+S_{ALK}} .X_H$
7	Fermentation	$q_{fe} \frac{K_{O2H}}{K_{O2H}+S_{O2}} \frac{K_{NOxH}}{K_{NOxH}+S_{NO}} \frac{S_F}{K_{fe}+S_F} \frac{S_{ALK}}{K_{ALK}+S_{ALK}} .X_H$
8	Lysis	$b_H X_H$
Nitrifying organisms, autotrophic (Ammonia oxidizing bacteria): X_{AOB}		
9	Aerobic growth of X_{AOB}	$\mu_{AOB} \frac{S_{O2}}{K_{O2AOB}+S_{O2}} \frac{S_{NH4}}{K_{NH4AOB}+S_{NH4}} \frac{S_{PO4}}{K_{PANO}+S_{PO4}} \frac{S_{ALK}}{K_{ALKANO}+S_{ALK}} .X_{AOB}$
10	Lysis	$b_{AOB} X_{AOB}$
Nitrifying organisms, autotrophic (nitrite oxidizing bacteria): X_{NOB}		
11	Aerobic growth of X_{NOB}	$\mu_{NOB} \frac{S_{O2}}{K_{O2NOB}+S_{O2}} \frac{S_{NH4}}{K_{NH4NOB}+S_{NH4}} \frac{S_{PO4}}{K_{PANO}+S_{PO4}} \frac{S_{ALK}}{K_{ALKANO}+S_{ALK}} .X_{NOB}$
12	Lysis	$b_{NOB} X_{NOB}$
Hydrolysis process		
13	Aerobic hydrolysis	$K_h \eta \frac{S_{O2}}{K_{O2S}+S_{O2}} \frac{X_S/X_H}{K_{XS}+X_S/X_H} .X_H$
14	Anoxic hydrolysis	$K_h \eta_{NOXS} \frac{K_{O2S}}{K_{O2S}+S_{O2}} \frac{S_{NOX}}{K_{NO3S}+S_{NOX}} \frac{X_S/X_H}{K_{XS}+X_S/X_H} .X_H$
15	Anaerobic hydrolysis	$K_h \eta_{fe} \frac{K_{O2S}}{K_{O2S}+S_{O2}} \frac{K_{NOXS}}{K_{NOXS}+S_{NOX}} \frac{X_S/X_H}{K_{XS}+X_S/X_H} .X_H$
Phosphorus accumulating organisms (PAO): X_{PAO}		
16	Storage of X_{PHA}	$q_{PHA} \frac{S_A}{K_{APAO}+S_A} \frac{S_{ALK}}{K_{ALKPAO}+S_{ALK}} \frac{X_{PP}/X_{PAO}}{K_{PP}+X_{PP}/X_{PAO}} .X_{PAO}$
17	Aerobic storage of X_{PP}	$q_{PP} \frac{S_{O2}}{K_{O2PAO}+S_{O2}} \frac{S_{PO4}}{K_{PS}+S_{PO4}} \frac{S_{ALK}}{K_{ALKPAO}+S_{ALK}} \frac{X_{PHA}/X_{PAO}}{K_{PHA}+X_{PHA}/X_{PAO}} \frac{K_{MAX}-X_{PP}/X_{PAO}}{K_{IPP}+K_{MAX}-X_{PP}/X_{PAO}} .X_{PAO}$
18	Anoxic storage of X_{PP}, denitrification (S_{NO2})	$\rho_{17} \eta_{NOXPAO} \frac{K_{O2PAO}}{S_{O2}} \frac{S_{NOX}}{K_{NOXPAO}+S_{NOX}} \frac{S_{NO2}}{S_{NOX}}$
19	Anoxic storage of X_{PP}, denitrification (S_{NO3})	$\rho_{17} \eta_{NOXPAO} \frac{K_{O2PAO}}{S_{O2}} \frac{S_{NOX}}{K_{NOXPAO}+S_{NOX}} \frac{S_{NO3}}{S_{NOX}}$
20	Aerobic growth of X_{PAO}	$\mu_{PAO} \frac{S_{O2}}{K_{O2PAO}+S_{O2}} \frac{S_{NH4}}{K_{NH4PAO}+S_{NH4}} \frac{S_{PO4}}{K_{PPAO}+S_{PO4}} \frac{S_{ALK}}{K_{ALKPAO}+S_{ALK}} \frac{X_{PHA}/X_{PAO}}{K_{PHA}+X_{PHA}/X_{PAO}} .X_{PAO}$
21	Anoxic growth of X_{PAO}, denitrification (S_{NO2})	$\rho_{20} \eta_{NOXPAO} \frac{K_{O2PAO}}{S_{O2}} \frac{S_{NOX}}{K_{NOXPAO}+S_{NOX}} \frac{S_{NO2}}{S_{NOX}}$

(*Continued*)

Table 1 (*Continued*)

j	Process	Process rate equation $\rho_j, \rho_j \geq 0$ $(M_1\ L^{-3}\ T^{-1})$
22	Anoxic growth of X_{PAO}, denitrification (S_{NO3})	$\rho_{20}\eta_{NOXPAO}\frac{K_{O2PAO}}{S_{O2}}\frac{S_{NOX}}{K_{NOXPAO}+S_{NOX}}\frac{S_{NO3}}{S_{NOX}}$
23	Lysis of X_{PAO}	$b_{PAO}X_{PAO}$
24	Lysis of X_{PP}	$b_{PP}X_{PP}$
25	Lysis of X_{PHA}	$b_{PHA}X_{PHA}$

according to the program structure of PITSF-SEU reactor. When all the vectors $\frac{1}{C_{i,j}}(dC/dt)$ were approximately equal to zero, a steady state was observed. The integration was most perfect when time step is very small, but the computing time increased inversely with the size of time step. Conversely, too large time step would result in great errors and other numerical problem. Thus, one criterion for an upper boundary on time step is:

$$\Delta t \ll -C(t) \times (dC/dt)^{-1} \tag{17}$$

where Δt is time step. By combining Eqs. (1b) and (17), and neglecting the $M_{i,j}$, $N_{i,j}$ terms in the mass balance, resulted the maximum step size as shown below:

$$\Delta t \ll V_j \times C_{ij}/C_{2ij} + N_{ij}) = \varphi_{ij} \tag{18}$$

The term φ_{ij} is the mean residence time of component j in reactor component i at steady state.

3. Extension ASM2d model development

3.1. Two-step nitrification processes of X_{AOB} and X_{NOB}

Under aerobic state condition, S_{NH4} is oxidized to S_{NO2} by X_{AOB}; subsequently, S_{NO2} is oxidized to S_{NO3} by X_{NOB}. The two-step nitrification reactions were described by two Eqs. (process (9) and (11) in Table 1) of extension model.

3.2. Decreases of S_{NO2} and S_{NO3} related to X_H

In ASM2d [16], it was assumed that S_{NO3} would be transformed directly into molecular nitrogen (N2) under anoxic state condition. Two types of carbon sources were utilized for the decreasing of S_{NO3}, including readily biodegradable substrate (S_F) and fermentation products (S_A). To describe these observing, two equations were adopted in ASM2d [17]. Indeed, nitrate (S_{NO3}) may be reduced to nitrite (S_{NO2}) and subsequently to molecular N_2 by heterotrophic bacteria (X_H) under anoxic state condition. In extension model, decreases of S_{NO2} and S_{NO3} using different carbon sources, whereas readily biodegradable fermentable organic substrate (S_F) and volatile fatty acids (S_A) were considered. As a result, four process Eqs. (process (3–6) in Table 1) were adopted to describe denitrification process in the extension model under anoxic state condition.

3.3. Decreases of S_{NO2} and S_{NO3} related to X_{PAO}

Previous studies reviewed that nitrite (S_{NO2}) also served as the electron acceptors for polyphosphate-accumulating organisms under anoxic state condition excepting nitrate (S_{NO3}) [2]. In extension of ASM2d model, it was assumed that the contribution of X_{PAO} for reducing nitrite and nitrate depended on the ratios of S_{NO2} and S_{NO3} to S_{NOX}.

3.4. Heterotrophic nitrification modeling

In PITSF process, SND process was clearly observed in tank two and tank three during phase II and III, respectively, whereas it was operated under a companied effect of nitrification and denitrification as shown in our previous work [1]. Thus, the stoichiometric matrix and process rate equation for both aerobic and anoxic conditions were considered for simulated each compound in these tanks. It is evident from this model (SND model) that two types of carbon sources (S_F and S_A) were modeled separately for reducing nitrate and nitrite under anoxic conditions, and therefore, four process Eqs. (process 3–6) in Table 1), and two types of carbon sources (S_F and S_A) were considered under aerobic condition (process (1) and (2) in Table 1).

Table 2
Stoichiometric matrix

No.	Process	S_F	S_A	S_{NH4}	S_{NO2}	S_{NO3}	S_{PO4}	S_I	S_{ALK}	X_S	X_H	X_{PAO}	X_{AOB}	X_{NOB}	X_{PP}	X_{PHA}	X_I	X_{TSS}
1	Aerobic growth on S_F	$-\frac{1}{Y_H}$		$V_{1,NH4}$			$V_{1,PO4}$				1							
2	Aerobic growth on S_A		$-\frac{1}{Y_H}$	$V_{2,NH4}$			$V_{2,PO4}$				1							
3	Anoxic growth on S_F, denitrification (S_{NO2})	$-\frac{1}{Y_H}$		$V_{3,NH4}$	$-\frac{1-Y_H}{1.71Y_H}$		$V_{3,PO4}$				1							
4	Anoxic growth on S_F, denitrification (S_{NO3})	$-\frac{1}{Y_H}$		$V_{4,NH4}$		$-\frac{1-Y_H}{2.86Y_H}$	$V_{4,PO4}$				1							
5	Anoxic growth on S_A, Denitrification (S_{NO2})		$-\frac{1}{Y_H}$	$V_{5,NH4}$	$-\frac{1-Y_H}{1.71Y_H}$		$V_{5,PO4}$				1							
6	Anoxic growth on S_A, denitrification (S_{NO3})		$-\frac{1}{Y_H}$	$V_{6,NH4}$		$-\frac{1-Y_H}{2.86Y_H}$	$V_{6,PO4}$				1							
7	Fermentation	−1	1	$V_{7,NH4}$			$V_{7,PO4}$											
8	Lysis			$V_{8,NH4}$			$V_{8,PO4}$				$1-f_{XI}$		−1					
f_{XI}																		
Nitrifying organisms, autotrophic (Ammonia oxidizing bacteria): X_{AOB}																		
9	Aerobic growth of X_{AOB}			$V_{9,NH4}$	$-\frac{1}{Y_{AOB}}$		$-i_{PBM}$						1					
10	Lysis			$V_{10,NH4}$			$V_{10,PO4}$				$1-f_{XI}$				−1			
f_{XI}																		
Ntrifying organisms, autotrophic (nitrite oxidizing bacteria): X_{NOB}																		
11	Aerobic growth of X_{NOB}			$V_{11,NH4}$	$-\frac{1}{Y_{NOB}}$	$-\frac{1}{Y_{NOB}}$	$-i_{PBM}$							1				
12	Lysis f_{XI}			$V_{12,NH4}$			$V_{12,PO4}$				$1-f_{XI}$					−1		
Hydrolysis process:																		
13	Aerobic hydrolysis	$1-f_{SI}$		$V_{13,NH4}$				f_{SI}	$V_{13,Alk}$	−1								$V_{13,Tss}$
14	Anoxic hydrolysis	$1-f_{SI}$		$V_{14,NH4}$				f_{SI}	$V_{14,Alk}$	−1								$V_{14,Tss}$
15	Anaerobic hydrolysis	$1-f_{SI}$		$V_{15,NH4}$				f_{SI}	$V_{15,Alk}$	−1								$V_{15,Tss}$
Phosphorus accumulating organisms (PAO) : X_{PAO}																		
16	Storage of X_{PHA}		−1				Y_{PO4}								Y_{PO4}	1		
17	Aerobic storage of X_{PP}						−1								1	$-Y_{PHA}$		
18	Anoxic storage of X_{PP} denitrification (S_{NO2})				$V_{18,NO2}$		−1								1	$-Y_{PHA}$		
19	Anoxic storage of X_{PP} denitrification (S_{NO3})					$V_{19,NO3}$	−1								1	$-Y_{PHA}$		
20	Aerobic growth of X_{PAO}			$V_{20,NH4}$			$-i_{PBM}$					1				$-\frac{1}{Y_H}$		
21	Anoxic growth of X_{PAO} denitrification (S_{NO2})			$V_{21,NH4}$	$V_{21,NO2}$		$-i_{PBM}$					1				$-\frac{1}{Y_H}$		
22	Anoxic growth of X_{PAO} denitrification (S_{NO3})			$V_{22,NH4}$		$V_{22,NO3}$	$-i_{PBM}$					1				$-\frac{1}{Y_H}$		
23	Lysis of X_{PAO}			$V_{23,NH4}$			$V_{23,PO4}$				$1-f_{XI}$			−1				
24	Lysis of X_{PP}						1								−1		f_{XI}	
25	Lysis of X_{PHA}		1													−1		

4. Results and discussion

4.1. Investigation results

In this study, certain information regarding the raw wastewater characteristics was provided from a main manhole of southeast university in Wuxi city (China). Four testing runs with different operations were used for model calibration and parameter estimation and also four different runs for model simulation. Their values are shown in Table (4). According to OUR experiments, the values of the maximum growth rates of X_H, X_{AOB}, and X_{NOB} were 6.0, 1.4, and 0.4 day^{-1}, respectively. Their rate constants for lysis and decay were 0.4, 0.08, and 0.04 day^{-1}, respectively.

4.2. Sensitivity analysis (SN) and model calibration

The effects of frequently large uncertainties parameters in PITSF-SU process should be taken into account before starting in the simulation of this system via sensitivity analysis. The sensitivity (SN) of effluent components for some important parameters was analyzed based on 8% change of the standard values. All stoichiometric are five parameters and kinetic parameters are 52 parameters of the extension model. The influent components are 16 parameters including the influent flow rate, external flow of sludge recycles (two parameters). The sensitivity analysis of the above parameters (ξ) according to output components (β) was calculated by the following formula [18].

$$(\mathrm{SN}) = (d\beta/\beta)/(d\xi/\xi) \tag{19}$$

where ($d\xi$) is the change in the parameter value ξ and $d\beta$ the change in the output β. According to sensitivity analysis, the output concentrations (β) have different sensitivities toward different parameters. This study showed that the effluent S_S of COD fraction observed to have a sensitivity of more than one (SN > 1) toward three parameters of μ_H, b_H, Y_H. It was also revealed that the effluent concentration of S_{NH4}, S_{NO2}, and S_{NO3} had a sensitivity of more than one (SN > 1) towards five (input S_{NH4}, μ_{AOB}, q_{pp}, Y_{AOB}, Y_{PO4}), eight parameters (μ_{AOB}, μ_{NOB}, μ_{PAO}, q_{pp}, Y_H, Y_{AOB}, Y_{NOB}, Y_{PO4}), and four parameters influent flow rate (μ_{AOB}, Y_H, Y_{PO4}), respectively. The effluent phosphate ($S_{PO4)}$ was mainly sensitive toward seven parameters (S_{PO4}, q_{PHA}, q_{pp}, μ_{PA0}, K_{MAX}, Y_H, and Y_{PO4}. The internal concentrations of S_S, S_{NH4}, S_{NO2}, S_{NO3}, and S_{PO4} were also sensitive for the stoichiometric and kinetic parameters at the end of the anaerobic tank. Additionally, this work showed that 59 kinetic parameters gave a sensitivity of more than one (SN > 1) according to the internal concentrations. According to the sensitivity analysis, the main parameters in activated sludge models are known to be approximately constant in domestic wastewater, the default values from previous studies [2] were used as shown in Table 3.

After analysis, the parameters of the model, the simulation data were calibrated to adjust coefficient values of the extension model, and thus, the simulation result by this model with these coefficients closely agree with the measured data. The model parameters are greatly dependent on environmental state conditions. The parameter values are estimated by minimizing the sum of squares (R^2) of the deviations between the experimental data and the model predictions with the objective function. The standard deviation for parameter calculation was required to be lower than 50% to ensure the validity of the parameters value obtained. An initial guess of these parameters is necessary to initiate the calibration procedure. To simplify the calibration process, it is desired to change as few constants as possible, because of the limited variability of some parameters. The selection of the parameters for calibration is mainly based on the result of sensitivity analysis.

4.3. Model validation

4.3.1. Simulation of soluble components

The model evaluation is performed from the comparison between the measured and predicated values. The experimental data of four related runs real domestic wastewater are used for extension model evaluation. The simulated and experimental NH_4^+-N, NO_3^-–N, and PO_4–P values of tank one, tank two, tank three, tank four, and tank five under different runs with a C/N ratio of (5.4, 6.7, 3.4, and 9.1) and C/P ratio of (45.2, 130.4, 27.63, and 52.23), respectively, as shown below:

4.3.1.1. Model validation of tank one. Fig. 6 shows the observed and predicated data of ammonia–N nitrate–N, and PO_4^-–P concentration of tank one under different runs. It has a good agreement between the observed and predicated data, whereas the sum of squares of the deviations (R_2) of NH_4^--N, PO_4–P, and NO_3^-–N were 0.98, 0.99, and 0.97, respectively, at run 1, 0.98, 0.99, and 0.98, respectively, at run 2, 0.99, 0.98, and 0.97, respectively, at run 3 and 0.99, 0.99, and 0.97, respectively, at run 4.

Under anoxic condition, it was found from Fig. 6 that NH_4^--N concentration was increased to 9.08, 9.6, 11.1, and 4.9 mg/L in runs 1, 2, 3, and 4, respectively,

Table 3
Definition and typical values for kinetic parameters

Item	Description	20°C	Units
Heterotrophic organisms: X_H			
μ_H	Maximum growth rate on substrate	6.00	g X_S g^{-1} X_H d^{-1}
q_{fe}	Maximum rate for fermentation	3.3	g X_S g^{-1} X_H d^{-1}
η_{NO2H}	Reduction factor for denitrification (S_{NO2})	0.5	–
η_{NO3H}	Reduction factor for denitrification (S_{NO3})	0.6	–
b_H	Rate constant for lysis and decay	0.4	d^{-1}
K_{O2H}	Saturation/inhibition coefficient for oxygen	0.2	g O_2 m^{-3}
K_{FH}	Saturation coefficient for growth on S_F	4	g COD m^{-3}
K_{fe}	Saturation coefficient for fermentation on S_A	4	g COD m^{-3}
K_{AH}	Saturation coefficient for growth on acetate S_A	4	g COD m^{-3}
K_{NO2H}	Saturation/inhibition coefficient for S_{NO2}	0.5	g N m^{-3}
K_{NO3H}	Saturation/inhibition coefficient for S_{NO3}	0.5	g N m^{-3}
K_{NOxH}	Saturation/inhibition coefficient for S_{NO3}	0.5	g N m^{-3}
K_{NH4H}	Saturation coefficient for ammonium (nutrient)	0.05	g N m^{-3}
K_{PH}	Saturation coefficient for phosphate (nutrient)	0.01	g p m^{-3}
K_{ALK}	Saturation coefficient for alkalinity (HCO^{-3})	0.1	mole HCO^{-3} m^{-3}
Nitrifying organisms, autotrophic (Ammonia oxidizing bacteria) X_{AOB}			
μ_{AOB}	Maximum growth rate of X_{AOB}	1.4	d^{-1}
b_{AOB}	Decay rate of X_{AOB}	0.08	d^{-1}
K_{O2AOB}	Saturation/inhibition coefficient for oxygen	0.5	g O_2 m^{-3}
K_{NH4AOB}	Saturation coefficient for ammonium (nutrient)	1	g N m^{-3}
K_{ALKAOB}	Saturation coefficient for alkalinity (HCO^{-3})	0.5	mole HCO^{-3} m^{-3}
K_{PAOB}	Saturation coefficient for phosphorus (nutrient)	0.01	g P m^{-3}
Nitrifying organisms, autotrophic (Nitrite oxidizing bacteria) X_{AOB}			
μ_{NOB}	Maximum growth rate of X_{NOB}	0.4	d^{-1}
b_{NOB}	Decay rate of X_{NOB}	0.04	d^{-1}
K_{O2NOB}	Saturation/inhibition coefficient for oxygen	0.5	g O_2 m^{-3}
K_{NH4NOB}	Saturation coefficient for ammonium (nutrient)	0.01	g N m^{-3}
K_{NO2NOB}	Saturation coefficient for ammonium (nutrient)	0.5	g N m^{-3}
K_{ALKNOB}	Saturation coefficient for alkalinity (HCO^{-3})	0.5	mole HCO^{-3} m^{-3}
K_{PNOB}	Saturation coefficient for phosphorus (nutrient)	0.01	g P m^{-3}
Hydrolysis of particulate substrate: X_S			
K_h	Hydrolysis rate constant	3	d^{-1}
η_{NOxS}	Anoxic hydrolysis reduction factor	0.6	–
η_{fe}	Anaerobic hydrolysis reduction factor	0.4	–
K_{O2S}	Saturation/inhibition coefficient for oxygen	0.2	g O_2 m^{-3}
K_{NOxS}	Saturation/inhibition coefficient for nitrite and nitrate	0.5	g N m^{-3}
K_{XS}	Saturation coefficient for particulate COD	0.1	g X_S g^{-1} X_H
Phosphorus-accumulating organisms: X_{PAO}			
q_{PHA}	Rate constant for storage of X_{PHA} (base X_{PP})	3.3	g X_{PHA} g^{-1} X_{PAO} d^{-1}
q_{PP}	Rate constant for storage of X_{PP}	1.5	g X_{PHA} g^{-1} X_{PAO} d^{-1}
μ_{PAO}	Maximum growth rate of PAO	1.2	d^{-1}
η_{NOxPAO}	Reduction factor for anoxic activity	0.8	–
b_{PAO}	Rate for lysis of X_{PAO}	0.2	d^{-1}
b_{PP}	Rate for lysis of X_{PP}	0.2	d^{-1}
b_{PHA}	Rate for lysis of X_{PHA}	0.2	d^{-1}
K_{O2PAO}	Saturation/inhibition coefficient for oxygen	0.2	g O_2 m^{-3}
K_{NOxPAO}	Saturation coefficient for nitrate, S_{NO3}	0.5	g N m^{-3}
K_{APAO}	Saturation coefficient for acetate S_A	4	g COD m^{-3}
K_{NH4PAO}	Saturation coefficient for ammonium (nutrient)	0.05	g N m^{-3}
K_{PS}	Saturation coefficient for phosphorus in storage of PP	0.2	g P m^{-3}
K_{PPAO}	Saturation coefficient for phosphate (nutrient)	0.01	g P m^{-3}

(*Continued*)

Table 3 (*Continued*)

Item	Description	20℃	Units
K_{ALKPAO}	Saturation coefficient for alkalinity (HCO^{-3})	0.1	mole HCO^{-3} m^{-3}
K_{PP}	Saturation coefficient for poly-phosphate	0.01	g X_{PP} g^{-1} X_{PAO}
K_{MAX}	Maximum ratio of X_{PP}/X_{PAO}	0.34	g X_{PP} g^{-1} X_{PAO}
K_{IPP}	Inhibition coefficient for PP storage	0.02	g X_{PP} g^{-1} X_{PAO}
K_{PHA}	Saturation coefficient for PHA	0.01	g X_{PHA} g^{-1} X_{PAO}

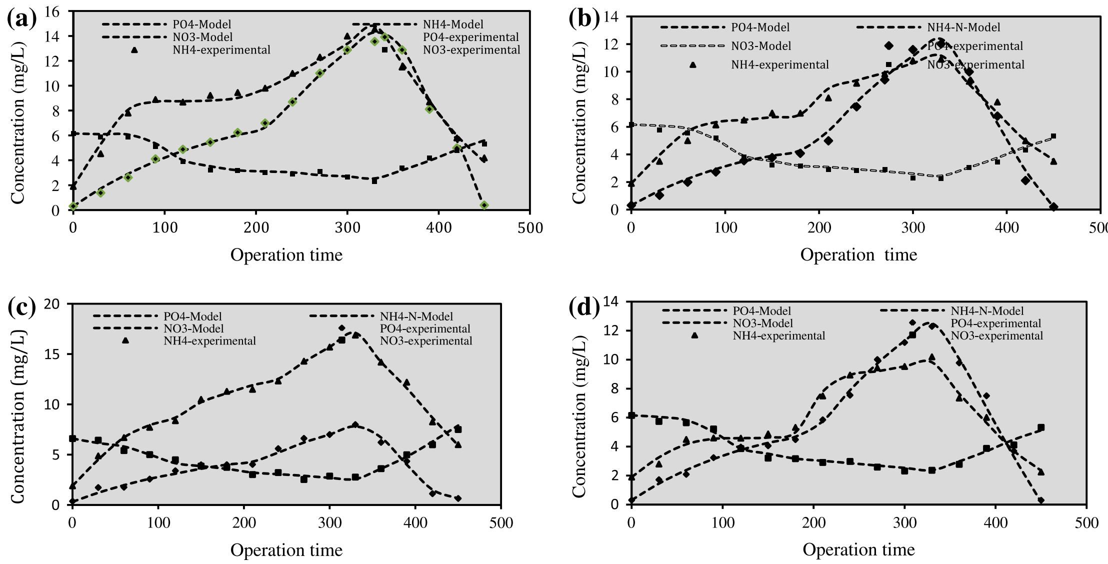

Fig. 6. Experimental data (points) and model simulation (lines) of NH_4-N, nitrate–N, and PO_4^-–P in tank one (a) run 1 (b) run 2 (c) run 3, and (d) run 4.

because NH_4^+–N concentration is decreased tendency with the increasing of C/N ratio (C/N is 9.1 in run 4). NO_3^-–N was decreased approximately to 3.1 mg/L in all runs of C/N ratio larger than five while it was decreased in run 3 due to an inadequate carbon source which led to insufficient denitrification process.

Under anaerobic condition during phase II, NH_4^+-N was increased to 17.4 mg/L in run 3, while it was increased to 9.8 mg/L in run 4 due to the increasing of C/N ratio.

Under aerobic condition during phase III, NH_4^+–N concentration was decreased below 4 mg/L during runs 1, 2, and 4 while it was decreased to 6 mg/L in run 4 due to low organic matter (C/N < 3.5) which required a long time for completion the nitrification process.

It can be seen clearly from Fig. 6, NO_3^-–N concentration was significantly increased and its increase rate gradually decreases with the increasing of C/N ratio. In the end of the aeration, NO_3–N concentration was 7.9 mg/L at low C/N ratio (run 3), while it was decreased to 5.6 mg/L at C/N ratio of 5.4, 6.7, and 9.1 in runs 1, 2, and 3, respectively. As can be seen from Fig. 6, PO_4^-–P concentration was released greatly to be 14.29 mg/L under anaerobic condition in run 1 and its releasing was decreased to be 7.99 mg/L in run 3. The proposed explanation for this observation is due to high VFA (S_A = 91) in run 1 and low VFA (S_A = 59) in run 4 which that effected significantly on phosphorus release. Under aerobic condition, phosphorus uptake in runs 1, 2, and 3 were better than run 4 owing to low C/P ratio in run 3 (C/P ratio was 27.6).

4.3.1.2. Model validation of tank two. Fig. 7 depicts the tested and predicated data of ammonia–N, nitrate–N, nitrite–N and PO_4^-–P concentrations of tank two under four investigated runs, This figure is shown a good consistency between the simulation values and test values, whereas the sum of squares of the deviations (R^2) of NH_4^+–N, PO_4^-–P, NO_2^-–N and NO_2^-–N were 0.99, 0.98,0.94, and 0.95, respectively, of at run 1, 0.99, 0.99, 0.98, and 0.99,

Table 4
Short definition of model component and typical raw wastewater characteristics

Symbol	Item	Unit	Run no.			
			1	2	3	4
Dissolved component						
S_O	Oxygen	g O2 m^{-3}	0	0	0	0
S_S	Readily biodegradable substrate	g COD m^{-3}	209	172	89	106
S_A	Volatile fatty acids	g COD m^{-3}	91	79	59	66
S_I	Inert soluble organic material	g COD m^{-3}	7.2	5.3	3.88	4.3
S_{NH4}	Ammonia nitrogen	g N m^{-3}	45.2	26.5	33	17.78
S_{NO2}	Nitrite nitrogen	g N m^{-3}	0.26	0.11	0.06	0.02
S_{NO3}	Nitrate nitrogen	g N m^{-3}	3.11	1.98	1.27	0.23
S_{ALK}	Alkalinity	mol HCO_3^- m^{-3}	4.83	5.23	4.93	5.11
S_{PO4}	Soluble orthophosphate	g P m^{-3}	5.83	1.49	4.26	3.55
Particulate component			1	2	3	4
X_I	Particulate inert organic material	g COD m^{-3}	61	59	53	57
X_S	Slowly biodegradable substrate	g COD m^{-3}	337	260	197	209
X_H	Active heterotrophic biomass	g COD m^{-3}	6	3	5	1
X_{AOB}	Ammonia oxidizing bacteria	g COD m^{-3}	0.5	0.1	0.3	0.01
X_{NOB}	Nitrite oxidizing bacteria	g COD.m^{-3}	0.08	0.01	0	0
MLSS (x_{TSS})	Mixed liquor suspended solid	g TSS m^{-3}	89	76	65	71

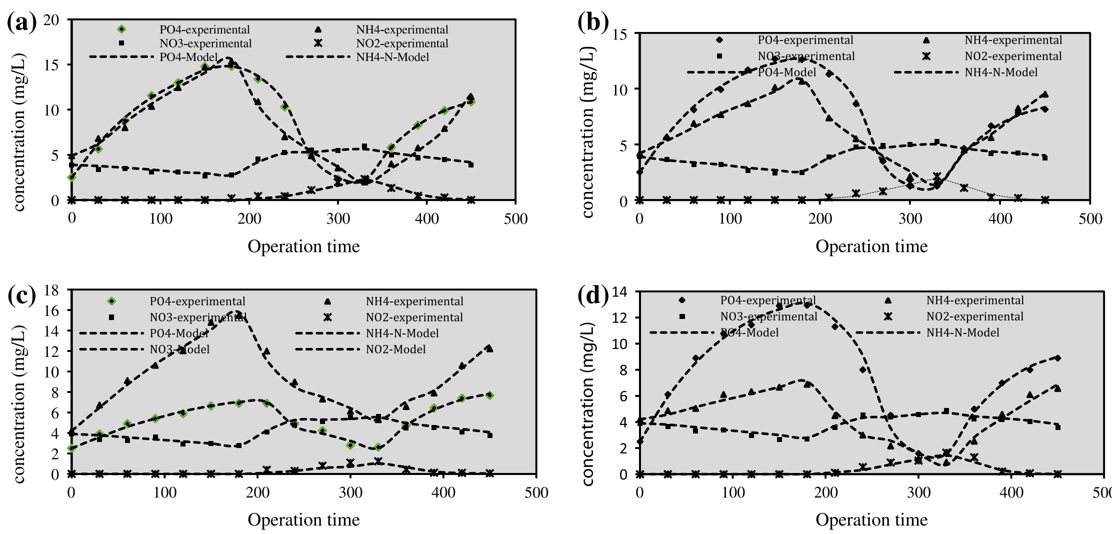

Fig. 7. Experimental data (points) and model simulation (lines) of different soluble components in tank two (a) run 1 (b) run 2 (c) run 3 and (d) run 4.

respectively, at run 2, 0.98, 0.98, 0.97, and 0.89, respectively, at run 3 and 0.98, 0.98, 9.99, and 0.92, respectively, at run 4. The analysis of biological reaction (denitrification and phosphorus release during phase I, nitrification and SND process during phase II and denitrification during phase III) were discussed previously. The main difference between the simulation result of the fourth runs were similar to the analysis to tank one, whereas NH_4^+-N was increased to 15.8 mg/L in run 3, while it was increased to 7.08 mg/L in run 4 due to insufficient organic matter in run 3. Under aerobic condition, it was concluded that all runs of $C/N > 4$ are more appropriateness that can met Chinese national class I (Grade A) sewage discharge standard. In PITSF process, SND process was clearly observed in tank two, whereas it was operated under a companied effect of nitrification and denitrification. The extension model was able successfully to simulate NO_3–N variation in tank two where the sum of squares of the deviations

(R^2) of NO_3–N was above 0.95 in all investigated runs.

It was notably from Fig. 7 that the indication of PO_4–P release and its uptake was similar to tank one. It was externally affected by VFA (Sa) variation in different runs. The simulation result showed that an extension model is a good development model to predicted NO_2–N pathway, whereas the sum of squares of the deviations R^2 of NO_2–N was (0.97) between the observed and predicted values.

4.3.1.3. Model validation of tank three. Fig. 8 shows the tested and predicated data of ammonia–N, nitrate–N, nitrite–N, and PO_4^-–P concentrations of tank three for four investigated runs. It showed a good reliability between the observed and predicated data, whereas the sum of squares of the deviations R^2 of ammonia–N, PO_4^-–P nitrate-N, and nitrite–N concentrations were 0.99, 0.98, 0.96, and 0.88, respectively, at run 1, 0.99, 0.97, 0.95, and 0.87, respectively, at run 2, 0.96, 0.99, 0.99, and 0.87, respectively, at run 3, and 0.99, 0.99, 0.95, and 0.84, respectively, at run 4. The aerobic denitrification phenomena (SND) were observed clearly during phase I. Thus, both anoxic and aerobic biological reaction is considered for each simulated compound. This model showed a good agreement to simulate the variation of NO_2–N and NO_3–N where NO_3–N concentration was decreased below 3 mg/L in run 4 (C/N > 7), while it was decreased slowly in run 3 due to low organic carbon which effected significantly on SND rate as shown previously [1].

4.3.1.4. Model validation of tank four. Fig. 9 depicts the observed and predicated data of ammonia–N, PO_4^-–P, and nitrite–N concentrations of tank four under four runs. It showed a good fitness between simulation and experimental data, whereas the sum of squares of the deviations (R^2) of NH_4^+–N, PO_4^-–P, and nitrite–N were 0.99, 0.94, and 0.97, respectively, at run 1, 0.98, 0.99, and 0.97, respectively, at run 2, 0.99, 0.99, and 0.98, respectively, at run 3, and 0.99, 0.98, and 0.98, respectively, at run 4. It was found from Fig. 9 that PO_4–P was decreased below 0.3 mg/L in runs 1, 2, 4, but it was decreased to 3.4 mg/L in run 3 due to low C/P ratio in this run. In spite of PO_4–P was consumed by X_{PAO} organism which utilized both S_{NO2} and S_{NO3} concentrations as a donor electron accepter, extension model is succeeded to model the variation of PO_4–P in phase I.

4.3.1.5. Model validation of tank five. Fig. 10 depicts the tested and predicated data of NH_4^+–N, PO_4–N, nitrate–N, and nitrite–N concentration of tank five under four investigated runs. This figure shows a good consistency between the observed and predicated data, whereas the sum of squares of the deviations (R^2) NH_4^+–N, PO_4–P, nitrate–N, and nitrite–N concentration of tank five were 0.91, 0.77, 0.99, and 0.77, respectively, at run 1, 0.92, 0.90, 0.99, and 0.71, respectively, at run 2, 0.99, 0.95, 0.77, and 0.68, respectively, at run 3, and 0.95, 0.73, 0.99, and 0.76, respectively, at run 4.

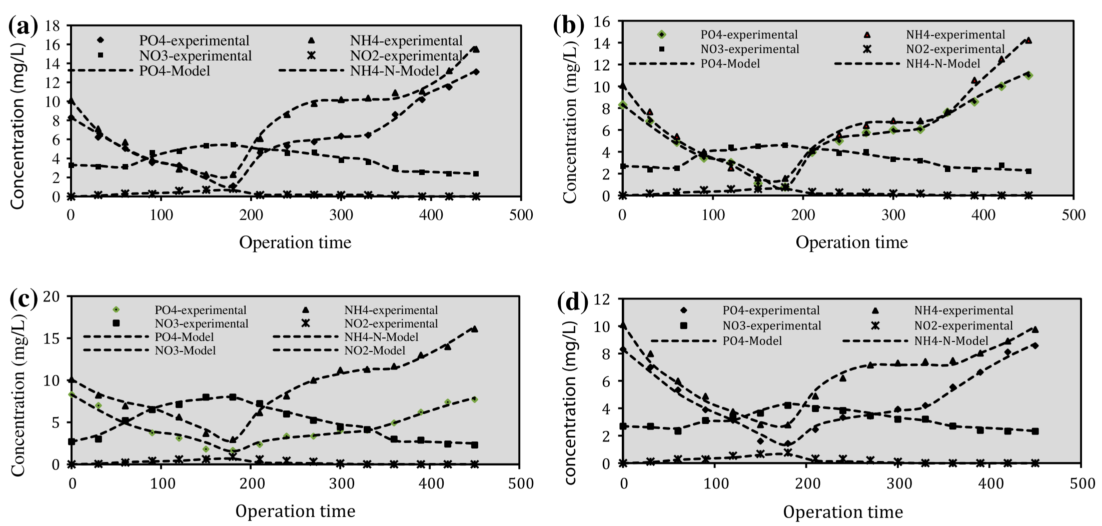

Fig. 8. Experimental data (points) and model simulation (lines) of different soluble components in tank three (a) run 1 (b) run 2 (c) run 3, and (d) run 4.

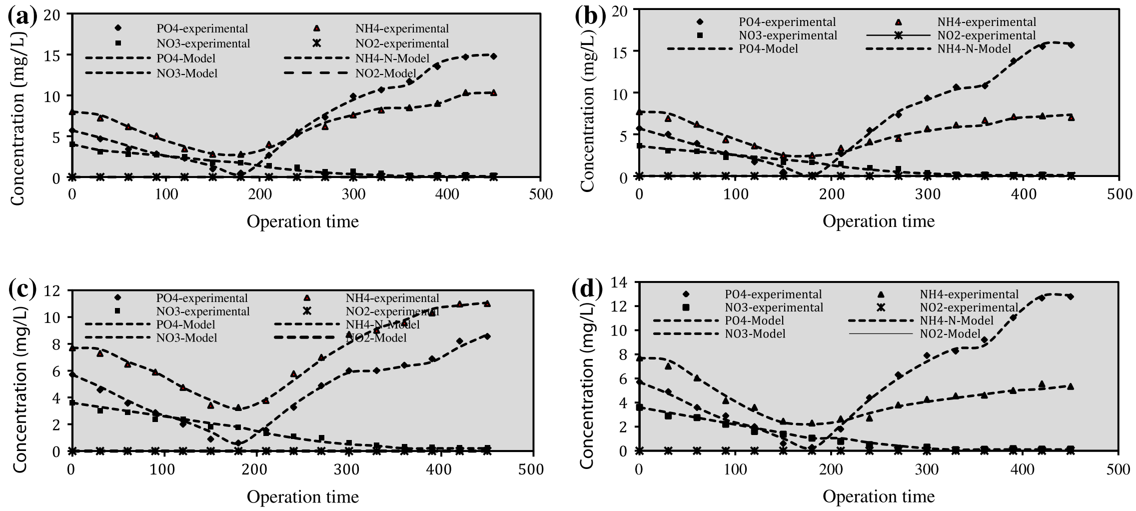

Fig. 9. Experimental data (points) and model simulation (lines) of different soluble components in tank four (a) run 1 (b) run 2 (c) run 3, and (d) run 4.

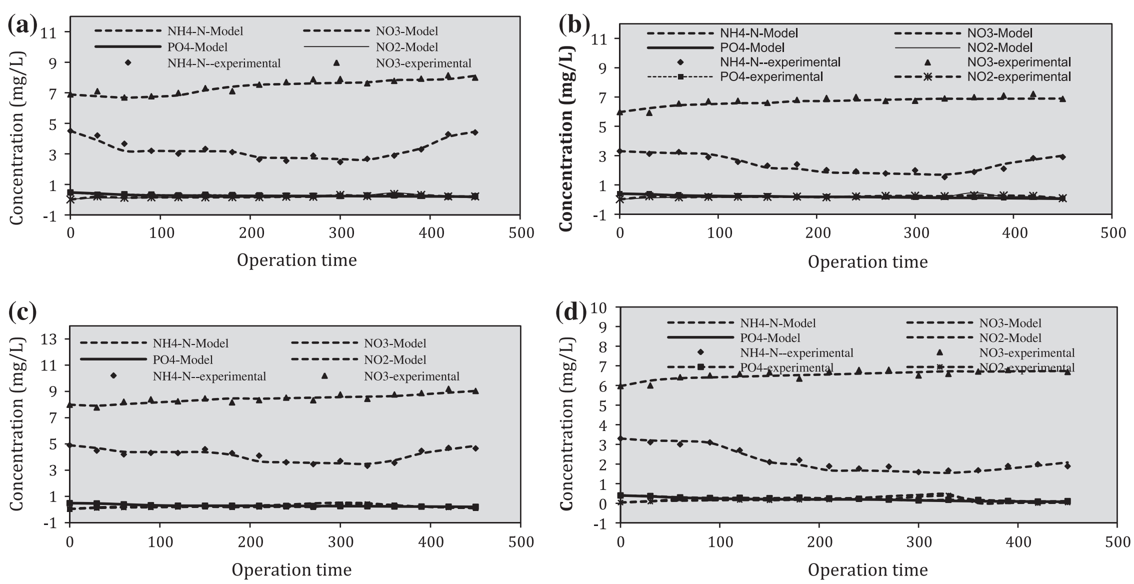

Fig. 10. Experimental data (points) and model simulation (lines) of different soluble components in tank five (a) run 1 (b) run 2 (c) run 3, and (d) run 4.

It can be seen readily from Fig. 10 that NH_4^+–N was approximately stabilized at 2.44, 1.2, 3.5, and 1.44 mg/L in runs 1, 2, 3, and 4, respectively. PO_4–P concentration was below 0.07 mg/L in runs 1, 2, and 4 while it was 0.2 mg/L in run 3 due to low C/P ratio in this run. However, the simulation result showed a geed convergence with the observed result where it can be meet Chinese national class I (Grade A) sewage discharge standard.

4.4.2. Simulation of particulate components

In this study, the variations of micro-organisms were evaluated by extension model in each tank during the first half-cycle. Fig. 11a–e showed the simulation values of particulate component concentrations during the first half-cycle under different runs. It was depicted that, the X_H, X_{PAO}, $X_{PP,}$ X_{AOB}, and X_{NOB} concentrations were 687–2,108, 130–257, 158–227,

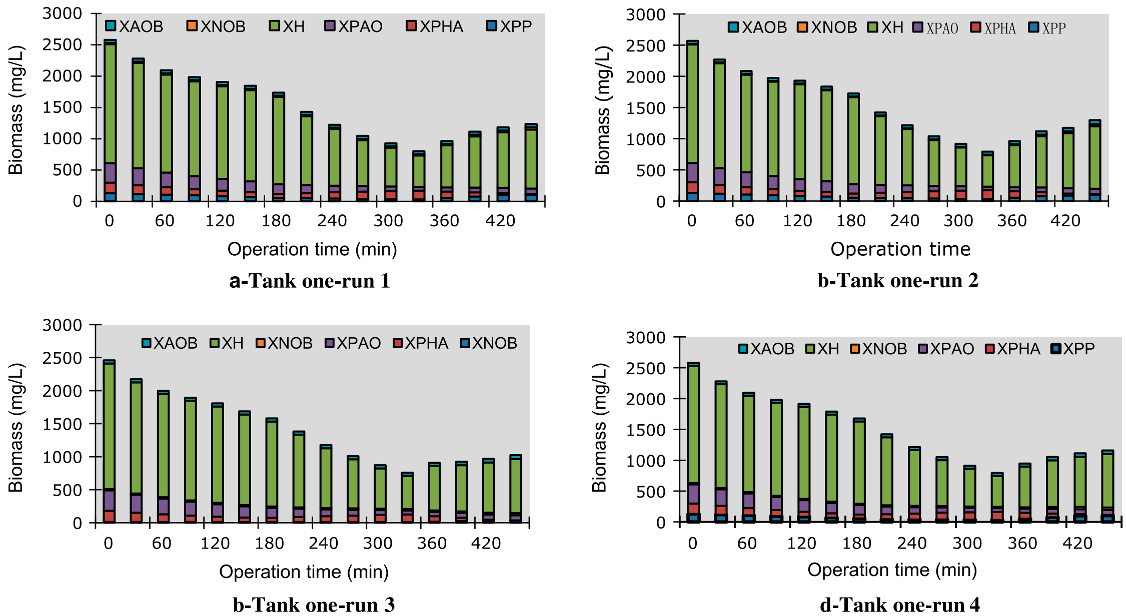

Fig. 11a. The biomass variations in tank one under different runs.

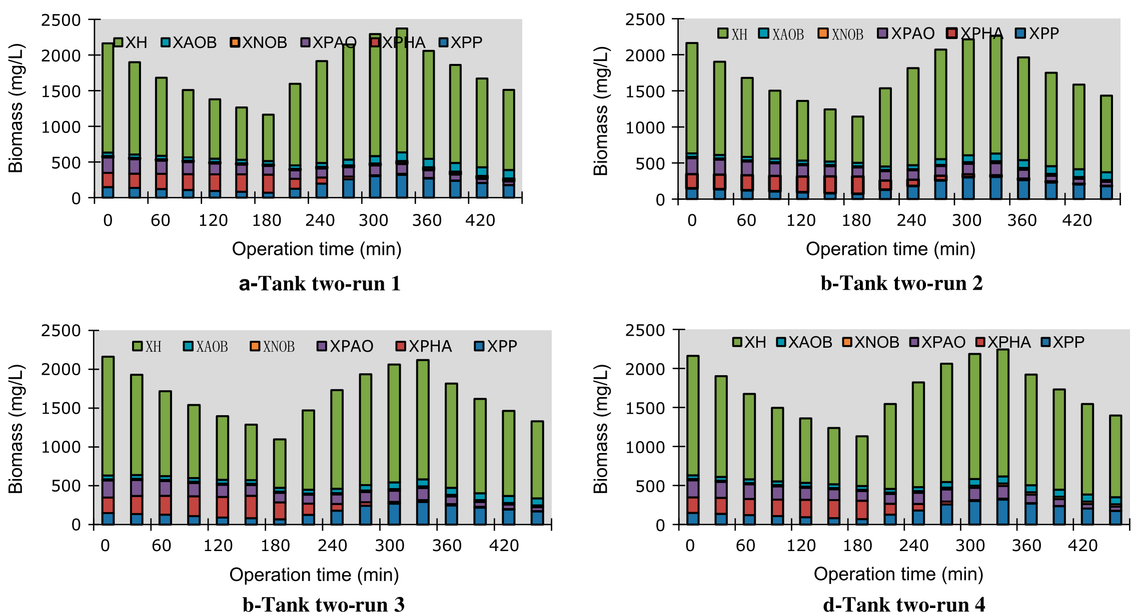

Fig. 11b. The biomass variations in tank one under different runs.

29–65, and 15–48 mg/L in PITSF-SEU process. According to Fig. 11a–e, X_H, X_{PAO}, X_{AOB}, and X_{NOB} were increased slowly with time in the anoxic tank, and then, it was decreased in the anaerobic tanks because of the lysis reaction. X_{PHA} were increased with time under anaerobic state condition tank due to phosphorus released, and then, it was decreased in the aerobic tanks due to phosphors uptake. The simulation result concluded that both X_{AOB} and X_{NOB} are utilized as an aerobic species that utilize free molecular oxygen as final electron accepter. Quantitatively, the particulate component of X_{AOB} was increased obviously to 66 mg/L in tank 1 under aerobic condition and X_{NOB} increased also to 36 mg/L in this tank due to aerobic growth. Although the particulate components of X_{AOB} and X_{NOB} varied in each

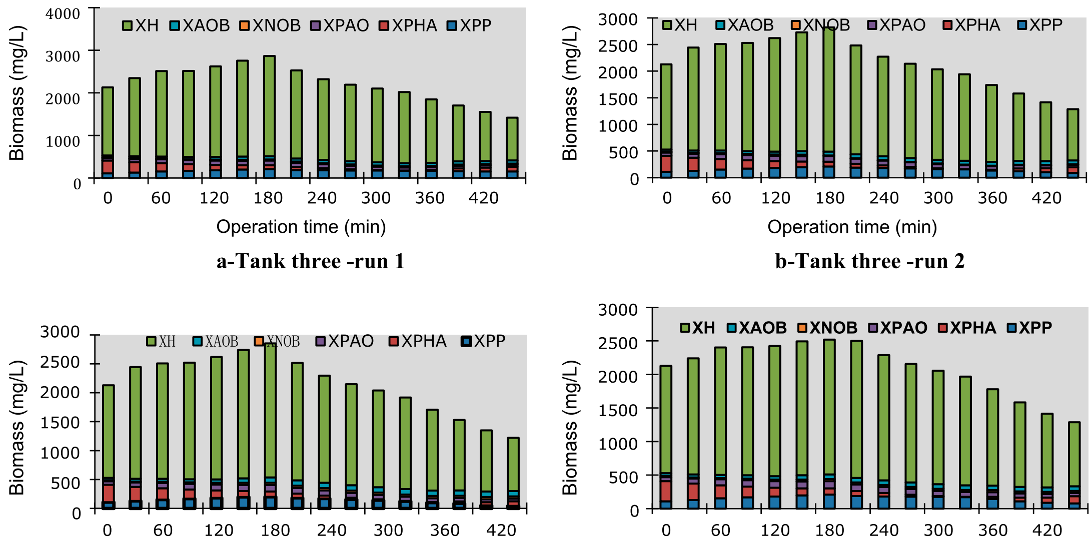

a-Tank three -run 1

b-Tank three -run 2

c-Tank three-run 3

d-Tank three-run 4

Fig. 11c. The biomass variations in tank three under different runs.

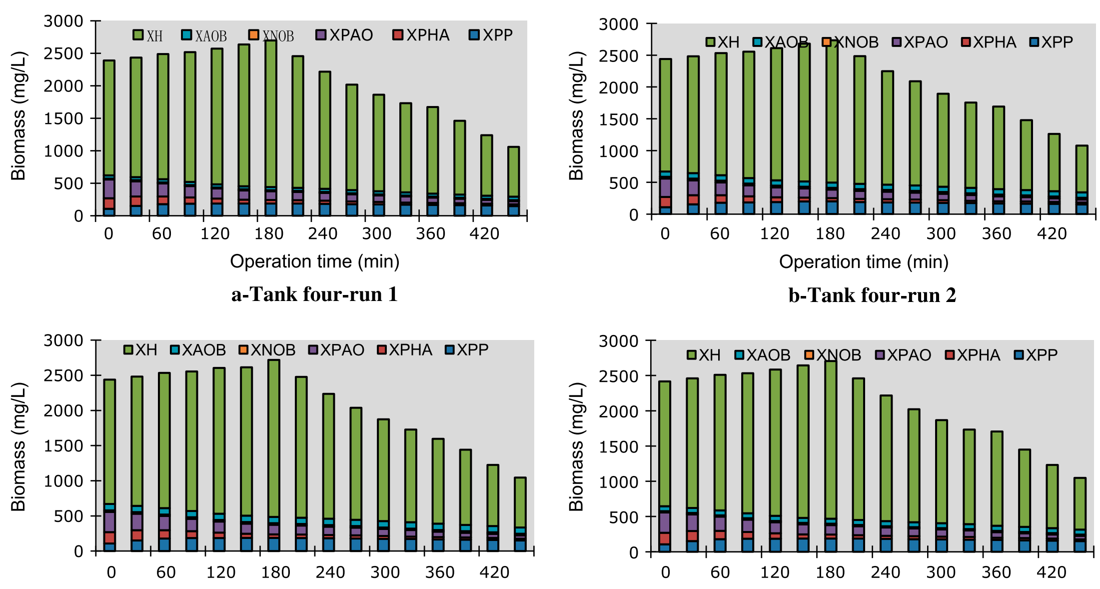

a-Tank four-run 1

b-Tank four-run 2

c-Tank four-run 3

d-Tank four-run 4

Fig. 11d. The biomass variations in tank four under different runs.

tank, the ratio of total nitrifying species to total active biomass was about 2–2.68% in each tank. Both X_H and X_{PAO} are facultative species that utilize free molecular oxygen or combined oxygen as final electron accepter for aerobic or anoxic growth. Quantitatively, the biomass of X_H was decreased to 1,393 mg/L in tank 1 (anoxic tank) in which the step feeding influent flowed during phase I, and then, it was decreased to 501 mg/L in phase II where tank 1 operated under anaerobic condition. It was increased obviously in phase III to be 942 mg/L. The particulate components of X_H, X_{PAO}, X_{PP}, X_{AOB}, and X_{NOB} increased in quantities by about 49, 27, 151, 88, and 98% in tank two due to change the environmental state condition

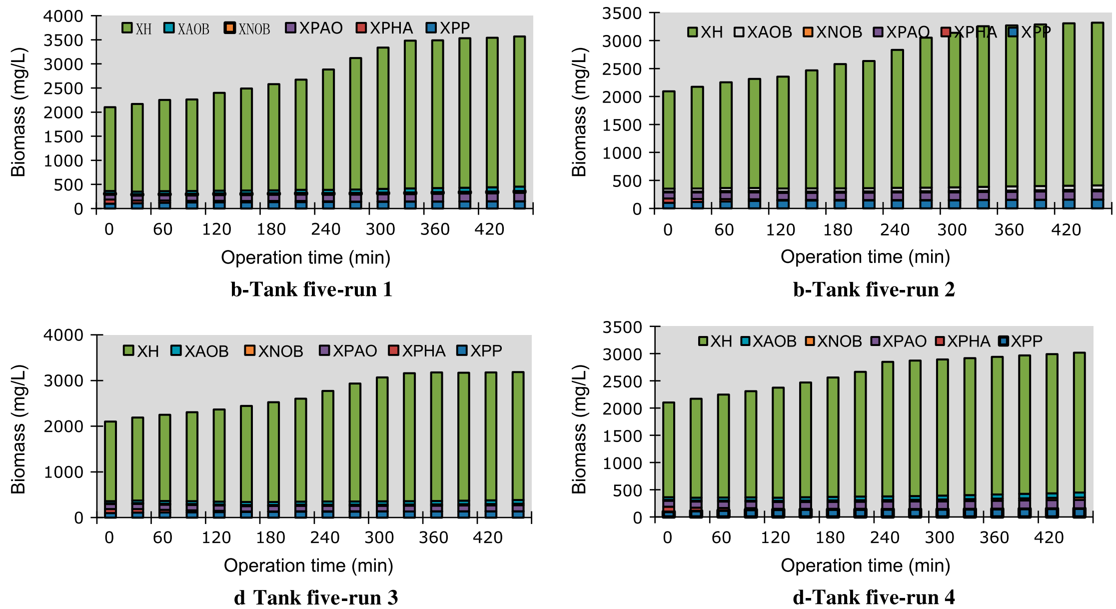

Fig. 11e. The biomass variations in tank five under different runs.

from anaerobic to aerobic during phase II and decreased in quantities by about 55, 67, 45, 0.11, and 0.4% in phase III due to change the environmental state condition from aerobic to anoxic in which the step feed influent pumped from tank 2 during this phase. The particulate components of X_{H}, X_{PAO}, $X_{PP,}$ X_{AOB}, and X_{NOB} increased slowly in quantities by about 41, 38, 37, 70.3, and 81% in whole phases of tank five because of the aerobic reaction as shown in Fig. 11a–e, while X_{PHA} was decreased in quantities by about 41%. In this study, the disadvantages of the developed biological nutrient removal processes were enhanced by reconfiguring the process without internal mixed liquor recirculation. This was done by configuring the process into five tanks with changeable environmental state condition into anaerobic/anoxic, aerobic zones in each tank to achieve optimum nutrient removal. In PITSF-SEU process, a step feed influent was also used to direct the influent into the anoxic tank as an external organic source for denitrification. Thus, the particulate components of X_{H}, X_{PAO}, and X_{PP} decreased in this tank due to the dilution effect of the second flow. The particulate components of X_{AOB} and X_{NOB} were also decreased due to the negative growth rate resulted from lysis reaction in the anoxic tank. In full-scale wastewater treatment plant, the transient system behavior is of high practical importance since variations of composition, influent flowrate as well as changes of operation prevents each real-world wastewater treatment plant from reaching the steady-state condition. Although the application of extension model under steady state was validated in this study, the application in transient state can be implemented in the future study. In addition, the practical applications of the extension model including plant controller layout, optimization, mathematical verification of the purification performance, and model-based state and parameter estimation should be taken into account in the future study.

5. Conclusions

The variation of soluble components of S_{NO2}, S_{NO3}, S_{NH4}, and S_{PO4} in PITSF-SEU process could be modeled successfully using an extension model. The results obtained in this work can be summarized as follows:

(1) The effective removal efficiency of ammonia–N, TN, and TP at 94%, 89.2%, 90.6%, respectively, were achieved effectively in PITSF-SEU process.

(2) In this study, μ_{AOB} and μ_{NOB} were 0.8 and 0.4 day^{-1}, respectively. Y_{AOB} was 0.18 and Y_{NOB} was 0.06. The values of (η_{NO2H}) and (η_{NO3H}) were chosen as 1.0 and 0.8, respectively.

(3) The simulation result showed a good agreement between the observed and predicated data, whereas the sum of squares deviations (R_2) of soluble components S_{NH4}, $S_{PO4,}$ S_{NO3} and S_{NO2} were more than 0.95 in all investigated runs. High NH_4^+-N and PO_4–P removal rate were achieved successfully in runs 1, 2, 4 of C/N

ratio > 5 and C/P ratio > 40.

(4) In this work, SND process was modified successfully in the first aerobic tanks during a main phase where both anoxic and aerobic biological reaction was considered for each compound.

(5) According to model simulation, X_H, X_{PAO}, X_{PP}, X_{AOB}, and X_{NOB} concentrations were 898–2,308, 104–244, 158–227, 22–69, and 13–48 in four test runs, respectively. The results concluded that the particulate components of X_H; X_{PAO}, X_{PP}, X_{AOB}, and X_{NOB} decreased in the anaerobic tanks because of the lysis reaction. Then, X_H; X_{PAO}, X_{PP}, X_{AOB}, and X_{NOB} increased in the aerobic tanks due to aerobic growth. They were increased in quantities by about 49, 27, 151, 88, and 98% in tank two due to change the environmental state condition from anaerobic to aerobic during phase II and decreased in quantities by about 55, 67, 45, 0.11, and 0.4% in phase III due to change the environmental state condition from aerobic to anoxic in which the step feed influent pumped from tank 2 during this phase.

Abbreviations

PITSF-SEU	—	phased isolation tank step feed-southeast university
A2/O	—	anaerobic–anoxic/oxic
SBR	—	sequence batch reactor
SND	—	simultaneous nitrification and denitrification
X_{AOB}	—	ammonia-oxidizing bacteria
X_{NOB}	—	nitrite oxidize bacteria
X_{PAOS}	—	phosphate-accumulating organisms
X_H, X_{PP}	—	poly phosphate organism heterotrophic organisms
PLC	—	programmable logic control
X_{PHA}	—	poly-hydroxylalkonates
OUR	—	oxygen uptake rate

References

[1] N. Rusul, A. Saad, X.W. Lu, Biological nutrient removal with limited organic matter using a novel anaerobic–anoxic/oxic multi-phased activated sludge process, Saudi J. Biol. Sci. 20(1) (2013) 1–21.

[2] M. Henze, W. Gujer, T. Mino, M.C.M. van Loosdrecht, Activated Sludge Models: ASM1, ASM2, ASM2d and ASM3, International Water Association, London, 2000.

[3] WEF, Biological and Chemical Systems for Nutrient Removal, Water Environment Federation, Alexandria, VA, 1999.

[4] J. Oles, P.A. Wilderer, Computer aided design of sequencing batch reactor based on IAWPRC activated sludge model, Water Sci. Technol. 23(6) (1999) 1087–1095.

[5] M. Henze, W. Gujer, Activated Sludge Model No. 2 IAWQ, Scientific and Technical Report No. 3 IAWQ, 1995, London, ISBN 9022200.

[6] M. Henze, W. Gujer, Activated Sludge Model No. 1 IAWPRC, Scientific and Technical Report No. 1 IAWQ, 1987, London, ISBN 1010-707X.

[7] M. Henze, W. Gujer, T. Mino, T. Matsuo, M.T. Wentzel, G.V.R. Marais, Activated Sludge Model No. 2 IAWQ, Scientific and Technical Report No. 3, IAWQ, 1995.

[8] M. Henze, W. Gujer, T. Mino, T. Matsuo, M.C. Wentzel, G.V.R. Marais, M.C. van Loosdrecht, Outline activated sludge model No. 2d, Water Sci. Technol. 39(1) (1999) 165–182.

[9] W. Gujer, M. Henze, T. Mino, M.C.M. van Loosdrecht, Activated sludge model no. 3, Water Sci. Technol. 39 (1) (1999) 183–193.

[10] G. Didem, K. Ozlem, B. Hanife, S. Seval, Storage phenomena in relation to carbon sources for denitrification, J. Desalin. Water Treat. 8(3) (2009) 171–176.

[11] J. Kappeler, R. Brodmann, Low F/M bulking and scumming: Towards a better understanding by modeling, Water Sci. Technol. 31(2) (1995) 225–339.

[12] S. Marsili-Libelli, F. Tabani, Accuracy analysis of a respirometer for activated sludge dynamic 351 modeling, Water Res. 36(11) (2002) 81–92.

[13] S.E.P.A. Chinese, Water and Wastewater Monitoring Methods, 4th ed., Chinese Environmental Science, Beijing, 2000.

[14] D. Mamais, D. Jenkins, P. Pitt, A rapid physico-chemical method for the determination of readily biodegradable soluble COD in municipal wastewater, Water Res. 27(1) (1993) 195–197.

[15] G. Philippe, A. Jean-Mark, U. Vincent, B. Jean-Claude, Estimation of nitrifying bacterial activities by measuring oxygen uptake in the presence of the metabolic inhibitors allylthiourea and azide, Appl. Environ. Microbiol. 64(3) (1998) 2266–2268.

[16] T. Mino, Activated Sludge Model: Microbiological Basis, in: G. Bitton (Ed.), Encyclopedia of Environmental Microbiology, 323(1), New York, NY, Wiley, 2002, pp. 14–26.

[17] D. Wild, R. Von Schulthess, W. Gujer, Structure modeling of denitrification intermediates, Water Sci. Technol. 31(2) (1995) 69–76.

[18] T.Y. Pai, S.H. Chuang, Y.P. Tsai, C.F. Ouyang, Modeling a combined A2O and RBC process under DO variation by using an activated sludge bio-film hybrid model, Environ. Eng. 130(12) (2004) 1433–1441.